Original Research

Magnetization-Prepared IDEAL bSSFP: A Flow-Independent Technique for Noncontrast-Enhanced Peripheral Angiography

Tolga Çukur, PhD,[1]* Ann Shimakawa, MS,[2] Huanzhou Yu, PhD,[2] Brian A. Hargreaves, PhD,[3] Bob S. Hu, MD, PhD,[4] Dwight G. Nishimura, PhD,[5] and Jean H. Brittain, PhD[6]

Purpose: To propose a new noncontrast-enhanced flow-independent angiography sequence based on balanced steady-state free precession (bSSFP) that produces reliable vessel contrast despite the reduced blood flow in the extremities.

Materials and Methods: The proposed technique addresses a variety of factors that can compromise the exam success including insufficient background suppression, field inhomogeneity, and large volumetric coverage requirements. A bSSFP sequence yields reduced signal from venous blood when long repetition times are used. Complex-sum bSSFP acquisitions decrease the sensitivity to field inhomogeneity but retain phase information, so that data can be processed with the Iterative Decomposition of Water and Fat with Echo Asymmetry and Least-Squares Estimation (IDEAL) method for robust fat suppression. Meanwhile, frequent magnetization preparation coupled with parallel imaging reduces the muscle and long-T_1 fluid signals without compromising scan efficiency.

Results: In vivo flow-independent peripheral angiograms with reliable background suppression and high spatial resolution are produced. Comparisons with phase-sensitive bSSFP angiograms (that yield out-of-phase fat and water signals, and exploit this phase difference to suppress fat) demonstrate enhanced vessel depiction with the proposed technique due to reduced partial-volume effects and improved venous suppression.

Conclusion: Magnetization-prepared complex-sum bSSFP with IDEAL fat/water separation can create reliable flow-independent angiographic contrast in the lower extremities.

Key Words: peripheral angiography; MR angiography; noncontrast enhanced; flow-independent; IDEAL; SSFP
J. Magn. Reson. Imaging 2011;33:931–939.

MAGNETIC RESONANCE ANGIOGRAPHY (MRA) of the extremities can help the diagnosis and monitoring of peripheral vascular diseases (PVD). Contrast-enhanced techniques have been the gold standard for MRA of the lower extremities in the last decade. However, PVD is one of the major risk factors for the development of renal artery stenosis and renal impairment (1), and the use of gadolinium-based contrast agents has recently been linked to nephrogenic systemic fibrosis in patients with chronic kidney disease (stage 4 and 5) and acute renal failure (2,3). The discovery of this link has led to renewed interest in noncontrast-enhanced MRA methods that can depict the peripheral vasculature without the injection of agents (4).

Noncontrast methods can be categorized into two groups: flow-dependent and flow-independent. Methods that belong to the former group, such as phase-contrast angiography (5), time-of-flight angiography (6), or fresh-blood imaging (7), exploit blood flow itself to selectively image the blood vessels. However, the flow rates and pulsatility can be significantly reduced with plaque formation or vascular occlusion. This reduces the ability of flow-dependent methods to accurately image the vessel morphology. On the other hand, flow-independent methods (8–10) can generate blood/background contrast even with slow flow in the extremities.

Flow-independent angiography (FIA) exploits the T_1, T_2, and chemical-shift differences among tissues to suppress background signals (8–10). Because balanced steady-state free precession (bSSFP) yields high signal-to-noise ratio (SNR) efficiency and bright blood signal (11), many FIA methods have focused on

[1]Helen Wills Neuroscience Institute, University of California, Berkeley, California, USA.
[2]MR Global Applied Science Laboratory, GE Healthcare, Menlo Park, California, USA.
[3]Department of Radiology, Stanford University, Stanford, California, USA.
[4]Cardiovascular Medicine, Palo Alto Medical Foundation, Palo Alto, California, USA.
[5]Department of Electrical Engineering, Stanford University, Stanford, California, USA.
[6]MR Global Applied Science Laboratory, GE Healthcare, Madison, Wisconsin, USA.
Contract grant sponsor: National Institutes of Health; Contract grant number: R01 HL039297, R01 HL075803; Contract grant sponsor: GE Healthcare.
*Address reprint requests to: T.Ç., Helen Wills Neuroscience Institute, 5107-B Tolman Hall, Berkeley, CA 94720.
E-mail: cukur@berkeley.edu
Received July 13, 2010; Accepted December 15, 2010.
DOI 10.1002/jmri.22479
View this article online at wileyonlinelibrary.com.

Table 1
The Proposed Strategy Combines Several Methods to Address the Issues That Compromise the Reliability of Flow-Independent bSSFP Angiograms

Method	Addressed issue(s)
Long-TR bSSFP	Arterial/venous contrast
Multipeak IDEAL	Fat suppression
Complex-sum bSSFP	Field inhomogeneity
Inversion recovery	Joint fluid and edema signals
T_2-preparation	Muscle and vein signals
Parallel imaging	Scan time

generating angiographic contrast with this sequence (12–16). Nevertheless, the reliability of bSSFP angiograms can be compromised by several factors: insufficient arterial/venous contrast, poor background suppression (for fat, long-T_1 fluids, and muscle), field inhomogeneity, and prolonged scan times due to large volumetric coverage.

In this work, we present a strategy to address these issues and produce high-spatial-resolution FIA angiograms with reliable blood/background contrast. The proposed method is based on a three-dimensional (3D) Cartesian bSSFP sequence with long repetition times (TRs) for improved arterial/venous contrast (17,18). Iterative Decomposition of Water and Fat with Echo Asymmetry and Least-Squares Estimation (IDEAL) (19,20) is used for suppressing the bright fat signal. Meanwhile, dual-acquisition complex-sum bSSFP (21) decreases the sensitivity to field inhomogeneity. Frequent magnetization preparation can effectively reduce the signals from long-T_1 fluids (i.e., $T_1 > 2000$ ms) and muscle, at the expense of increased scan time. Finally, parallel imaging is used to decrease the scan-time penalties from long TRs, dual acquisitions, and frequent preparation.

MATERIALS AND METHODS

A variety of potential solutions exist for each of the aforementioned problems affecting the quality of FIA angiograms. However, these individual solutions must be compatible with each other to simultaneously address the issues. Table 1 lists the unique set of elements combined in the proposed strategy and the corresponding issues they address. Detailed descriptions of these elements are provided in the following sections.

Long-TR bSSFP

Due to the small vessel diameters, peripheral angiograms are often acquired with high isotropic resolution over large fields-of-view (FOVs), mostly occupied by muscle tissue. Balanced SSFP sequences, which yield bright blood signal, can be used for collecting FIA datasets with high SNR efficiency (12–16). Fortunately, the lower T_2/T_1 ratio of muscle leads to decreased bSSFP signal compared with blood. The muscle signal can be further reduced by exploiting the increased magnetization-transfer effect at higher specific absorption rates (SARs) (22). This could be achieved by prescribing higher tip angles and shorter repetition times (TRs).

Although muscle constitutes the largest volume of background signal in the extremities, arterial/venous separation is more essential because pairs of deep veins course immediately adjacent to each artery. Arterial/venous contrast arises from the differences in blood oxygen saturation. It has been recently demonstrated that longer TRs and/or higher field strengths substantially improve this contrast for bSSFP sequences (17,18,22). In this work, we effectively reduce both the venous and muscle signals by coupling long TRs (~10 ms) with high tip angles (~90°).

Figure 1 shows the phase-cycled bSSFP spectral profiles of the arterial and venous blood at $\alpha = 90°$ for two different TRs: 5 and 10 ms. The simulations were performed using a T_1 of 1273 ms for both arterial and venous blood at 1.5 T (17). Assuming arterial blood has a T_2 of 254 ms relatively independent of TR (17), the apparent T_2 of venous blood was computed from the values of bSSFP arterial/venous contrast plotted as a function of TR at $\alpha = 60°$ in Hong et al (23): 206

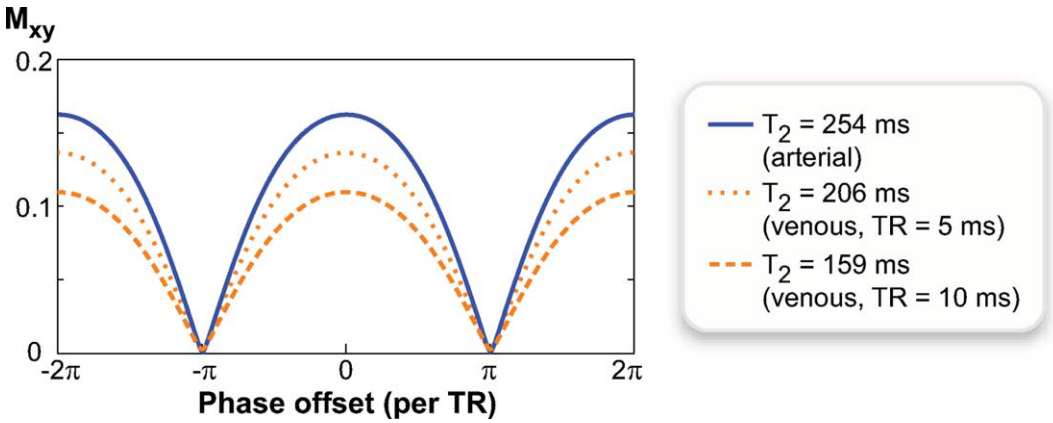

Figure 1. Increasing the imaging TR decreases the apparent T_2 of venous blood, and enhances the oxygen-dependent arterial/venous contrast in bSSFP sequences. The bSSFP spectral profiles for arterial and venous blood are shown for $\alpha = 90°$ and TR = 5, 10 ms. The arterial-blood profile ($T_2 = 254$ ms) remains the same for both TRs. On the other hand, the T_2 of venous blood drops from 206 ms (TR = 5 ms) to 159 ms (TR = 10 ms), yielding reduced signal. [Color figure can be viewed in the online issue, which is available at wileyonlinelibrary.com.]

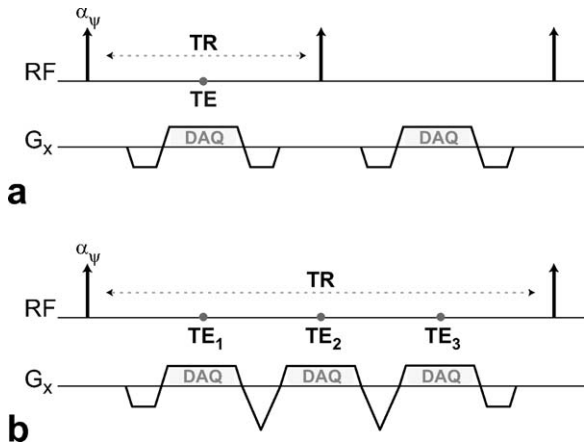

Figure 2. Diagrams showing the radio frequency excitations and the readout gradient waveforms of two bSSFP sequences. **a**: A single echo is acquired per TR. **b**: A multiecho flyback acquisition is performed each TR, where the gradients for all three echoes have the same polarity.

ms at TR = 5 ms, and 159 ms at TR = 10 ms. The percentage of oxygenated hemoglobin ($\%O_2$) was taken as 97% for arterial and 70% for venous blood in these computations (17,23). Whereas the on-resonant arterial/venous contrast is only 1.19 with TR = 5 ms, it increases to 1.49 with TR = 10 ms yielding a 25% improvement.

IDEAL Fat/Water Separation

Due to the larger T_2/T_1 ratio of fat, its bSSFP signal is higher than that for most water-based tissues (e.g., blood, muscle). Unless properly suppressed, the signal from intermuscular, subcutaneous, and bone-marrow fat can confound the angiograms. Furthermore, for some methods of bSSFP fat suppression, partial-volume effects can cause blood-signal loss in voxels concurrently occupied by fat and water (15). The level of suppression can be compromised by field inhomogeneity and/or partial-volume effects for most fat-suppression techniques previously proposed for noncontrast-enhanced bSSFP angiography (12,14–16).

In this work, we use IDEAL for reliable fat suppression in bSSFP images with minimal blood-signal loss (13,19,20,24). Figure 2 shows two different strategies of collecting the three echoes needed for IDEAL. We can simply acquire a single echo in each TR and vary the echo time (TE). Alternatively, all three echoes can be acquired within a single TR. Because long TRs are already required for improved venous suppression, the latter strategy is more efficient in terms of scan time. This multiecho sequence can be implemented with flyback readout gradients (25) as shown in Figure 2b, to avoid *k*-space misalignments and image-registration problems due to alternating gradient polarities (26).

Because the true fat spectrum has multiple peaks instead of a single peak at −220 Hz (for 1.5 Tesla [T]), the water images produced with regular IDEAL have residual fat signal. Nonetheless, IDEAL reconstructions can be generalized by including multiple resonant frequencies for fat, and estimating the relative amplitudes of these peaks with a self-calibrating approach (27). To enhance the quality of the angiograms, the fat suppression is further improved with a multipeak IDEAL reconstruction (27).

Complex-Sum bSSFP

The periodic signal nulls in the bSSFP profile, caused by off-resonance, can create banding artifacts in the reconstructed images. The lower extremities experience considerable field inhomogeneity due to their large volume and complicated geometries. The sensitivity to off-resonance is further increased with the use of long TRs. As a result, bSSFP acquisitions suffer from severe banding artifacts.

In addition to causing signal loss, banding artifacts can also reduce the robustness of the IDEAL reconstruction (28). Figure 3a displays the water (arterial blood) and fat profiles for TR = 10 ms, assuming a T_1/T_2 of 260/80 ms (29) and a chemical shift of −220 Hz for fat at 1.5 T. The profiles are not aligned because the null-to-null spacing of the bSSFP passbands is not a multiple of the fat-water frequency shift (28). Therefore, across a given signal null, the fat and water signals have significantly different phase and magnitude profiles.

We can suppress the banding artifacts by combining two acquisitions with different phase cycling (21,30). Figure 3 shows the profiles for (0–180)° and (0–0)° phase-cycled bSSFP sequences along with a complex summation of the two. Because complex-sum bSSFP perfectly preserves the relative phase differences between separate echo times, the residual ripples in the magnitude will not cause problems and the data can be directly reconstructed with IDEAL. The suppression of the banding artifacts also improves the robustness of the IDEAL reconstruction.

Magnetization Preparation

Long-T_1 fluids (i.e., $T_1 > 2000$ ms) such as joint fluid or edema have larger T_2/T_1 ratios than blood, and generate considerably higher bSSFP signals. Therefore, suppressing these signals is essential for visualizing the underlying vasculature, especially when these fluids have a diffuse distribution in the volume of interest (e.g., joint fluid in the feet). A nonselective adiabatic inversion-recovery (IR) pulse (31) can be used to reduce the long-T_1 signals, but the prepared contrast is transient and relatively T_2-independent. To minimize the duration and severity of the transient period following a preparation, we can first use a segmented adiabatic B_1-insensitive rotation (BIR-4) pulse (32) to induce T_2-weighting and approach the steady-state arterial/venous and blood/muscle contrast. Then, the tip angles of the bSSFP sequence can be gradually scaled with a Kaiser-Bessel design to avoid artifacts from transient oscillations (33). The k_y-k_z plane is divided into radial fan-beam segments that contain equal number of phase encodes (34). Because the energy in MR images is mostly concentrated at low spatial frequencies, the prepared magnetization

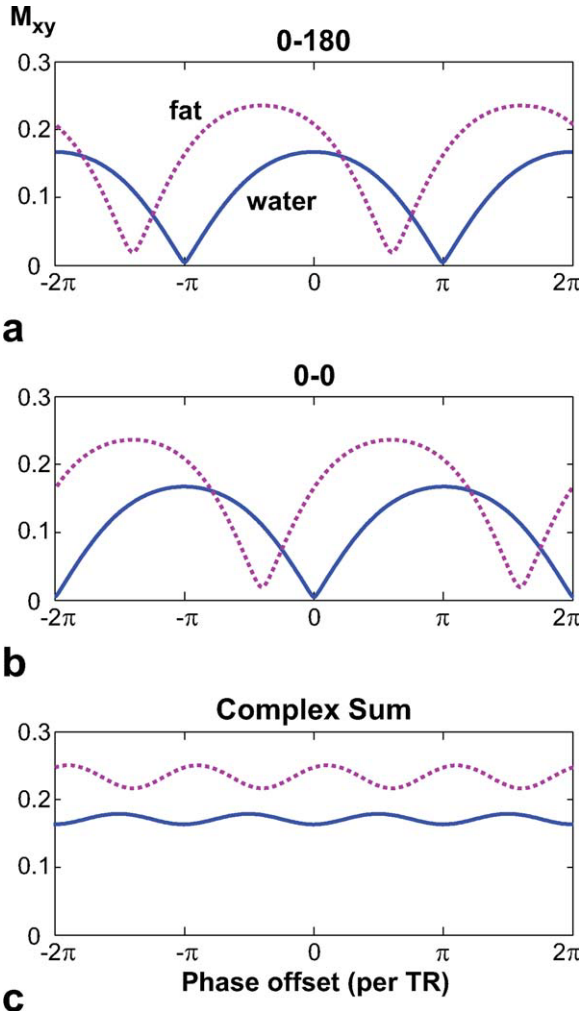

Figure 3. The spectral profiles of fat (dotted line, T_1/T_2 = 260/80 ms) and water (solid line, arterial blood - 1273/254 ms) are displayed for $\alpha = 90^\circ$ and TR = 10 ms, assuming a chemical shift of −220 Hz for fat at 1.5 T. The spectral axis represents the phase offset per TR due to field inhomogeneity only. **a**: For (0–180)° phase-cycling, the center of the fat and water profiles are not aligned. Therefore, the fat and water signals experience considerably different magnitude weightings around a signal null. This can lead to the failure of the IDEAL reconstruction. **b**: A (0–0)° phase-cycling shifts all profiles and the null locations in the frequency axis. **c**: A complex-summation of the two phase-cycled acquisitions removes the signal nulls to give nearly-flat profiles. Furthermore, IDEAL reconstructions can be directly applied on the resulting dataset because the phase differences are preserved.

can be captured more effectively by performing centric phase-encode ordering within each fan-beam segment (35). The magnetization is allowed to recover at the end of the segment, and the preparation is repeated before the next one.

Figure 4a displays the pulse sequence diagram for a single *k*-space segment. The resulting transient signal is shown in Figure 4b for arterial blood, venous blood, muscle (T_1/T_2 = 870/50 ms) (29), and joint fluid (2850/1210 ms) (36). The following parameters were used for the simulation: $\alpha = 90^\circ$; TR = 10 ms, 1.7-s IR time, 80-ms T_2-preparation time, and a 12-excitation catalyzation. The IR time was selected to minimize the joint-fluid signal for several seconds at the beginning of the acquisition, while the 80-ms T_2-preparation restored the arterial/venous and blood/muscle contrast approximately to their steady-state values.

Parallel Imaging

Covering a large volume with high spatial resolution requires significant scan time, especially when two magnetization-prepared long-TR bSSFP acquisitions are needed. Preparing the magnetization more frequently for improved contrast further increases the scan time. We undersampled the *k*-space acquisitions to avoid prolonged scan times due to frequent preparations. The missing data were recovered using the Autocalibrating Reconstruction for Cartesian sampling (ARC) (37) method, with data-driven calibration. By performing two-dimensional acceleration in the phase-encode plane, the number of encodes per *k*-space segment can be reduced while keeping the same number of segments. A greater portion of the encodes can then be acquired during the initial part of the transient-contrast curve, and the effect of magnetization preparation will be enhanced.

In Vivo Experiments

All experiments were performed with an 8-channel receive array on a 1.5 T GE Signa Twinspeed scanner

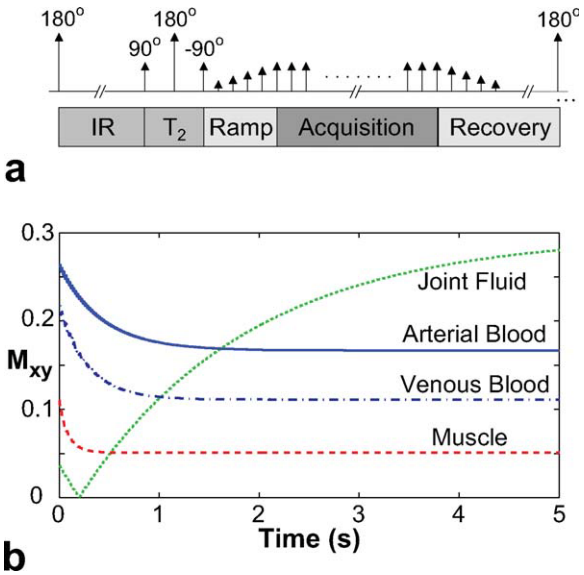

Figure 4. a: The pulse sequence diagram of a magnetization-prepared bSSFP sequence. The preparation section, which consists of inversion recovery, T_2-preparation, and catalyzation segments, is followed by bSSFP acquisitions. Afterward, the magnetization is allowed to recover, and the whole module is repeated to acquire the next *k*-space segment. **b**: The magnetization-prepared transient signals (i.e., during the acquisition period) for arterial blood (T_1/T_2 = 1273/254 ms), venous blood (1273/159 ms), muscle (870/50 ms), and joint fluid (2850/1210 ms).

(GE Healthcare, Waukesha, WI) with Zoom gradients (40 mT/m maximum strength and 150 T/m/s maximum slew rate). Our institutional review board approved the protocols used in these studies, and we obtained written informed consent from all participating subjects. The subjects were examined in supine position, and a superior–inferior readout direction was chosen along with anterior–posterior and right–left phase-encoding directions. The following parameters were prescribed for the 3DFT IDEAL bSSFP sequence: $\alpha = 90^\circ$, TR = 10 ms, 2.8-ms echo spacing, 1.7-s IR time, 80-ms T_2-preparation time, a 12-excitation catalyzation, 3-s recovery time, and 2.8-fold parallel-imaging acceleration. The total scan time was calculated as follows:

$$T_{scan} \cong 2 \cdot \left\{ N \cdot (T_{prep} + T_{rec}) + \frac{TR \cdot num_{PE}}{R} \right\},$$

where N is the number of *k*-space segments, T_{prep} and T_{rec} are the magnetization preparation and recovery times for a single segment, num_{PE} is the total number of phase encodes at the Nyquist sampling rate, and R is the acceleration factor.

While a 1.4-mm isotropic resolution was used for the thigh, this value was reduced to 1 mm in the calf and foot to compensate for the smaller vessel sizes. The number of phase encodes per *k*-space segment were 600 for the thigh (N = 19) and the calf (N = 38), and 300 for the foot (N = 32). The following FOVs were captured: 35 × 35 × 18 cm^3 (250 × 250 × 128 encoding matrix) in 6 min 28 s for the thigh, 31 × 28 × 14 cm^3 (310 × 280 × 140 matrix) in 8 min 15 s for the calf, and 27 × 19 × 14 cm^3 (270 × 190 × 140 matrix) in 8 min 14 s for the foot. The datasets were zero-padded by a factor of 2 in all three dimensions before maximum-intensity projections (MIPs) for improved visualization.

To demonstrate the effects of the individual elements in the proposed strategy, several foot angiograms were acquired with a different element added at each step. First, a reference angiogram was produced with a single-acquisition bSSFP sequence without any magnetization preparation. Two unprepared bSSFP acquisitions were then complex-summed to suppress the banding artifacts in the reference acquisition. Because approximately 10% of the fat signal is at the water frequency, residual fat signal will be observed in the water images with regular IDEAL. Therefore, a multipeak IDEAL reconstruction (27) was performed on the summation to improve the fat suppression. Next, magnetization preparation was performed with 900 phase encodes per segment (N = 11) to reduce the joint-fluid signal. Finally, the excitation cluster per preparation was reduced (300 encodes per segment, N = 32) to better capture the suppression.

Balanced SSFP angiograms of the calf and the foot were produced with IDEAL and another fat-suppression technique that is relatively immune to field inhomogeneity, phase-sensitive (PS) SSFP (38). IDEAL images were compared with PS-SSFP angiograms on three healthy volunteers (one female and two males; mean age of 30 ± 3 years; age range of 28–34 years), to show partial-volume and TR-related effects on the image contrast. PS-SSFP requires an optimal TR of 4.6 ms at 1.5 T and is more prone to partial-volume effects than IDEAL (38). To achieve a fair comparison between the techniques, we equated the total scan times and the acquisition times for each *k*-space segment by using different parallel-imaging accelerations. Because TR ≅ 5 ms for PS-SSFP and TR = 10 ms for IDEAL, the acceleration factors were 1.4 and 2.8, respectively.

The arterial/venous and blood/muscle contrast as well as blood SNR were measured in IDEAL and PS-SSFP angiograms. Paired, one-tailed Student's t-tests were performed on the measurements, and $P < 0.10$ was assumed to indicate statistical significance. Contrast was defined as the ratio of the mean signals, and SNR was computed as the ratio of the mean signal to the standard deviation of noise. The measurements were performed in identical regions of the source images with relatively homogeneous signal. These regions were selected to contain a minimum of 150 pixels. While the mean blood signal was estimated around the anterior tibial and dorsalis pedis arteries, adjacent muscle tissue was picked to quantify the background signal along with the noise variance.

To demonstrate the reliability of the generated angiographic contrast, the lower extremities of five healthy subjects (two females and three males; mean age of 34 ± 8 years; age range of 28–47 years) were scanned with the IDEAL method in three stations: the thigh, the calf and the foot. Inverse-video MIPs of the angiograms were computed for enhanced visualization.

RESULTS

The improvements obtained by the individual elements of the proposed strategy are demonstrated in Figure 5. A single-acquisition bSSFP image suffers from banding artifacts as expected, and fat/water separation is compromised with regular IDEAL around these artifacts (Fig. 5a). A complex-summation of two bSSFP datasets successfully removes the artifacts, and prevents the failure of IDEAL (Fig. 5b). A multipeak IDEAL reconstruction of this dataset achieves superior fat suppression, and the corresponding MIP clearly shows some vessels blocked by the remnant fat signal in the single-peak reconstruction (Fig. 5c). Finally, the bright joint-fluid signal can be reduced with the help of magnetization preparation (Fig. 5d), and increasing the frequency of preparation improves the background suppression at the expense of a 70% increase in scan time (Fig. 5e).

Figure 6 shows the lower-leg and foot angiograms produced with PS-SSFP and IDEAL. PS-SSFP yields a high and uniform level of fat suppression over the lower extremities, and relatively improved suppression of the joint-fluid in the knees, with a simpler reconstruction compared with IDEAL. However, at the prescribed resolutions, PS-SSFP is prone to partial-volume effects and causes blood-signal loss in small vessels. In contrast, IDEAL enhances the depiction of small vasculature. IDEAL also achieves improved

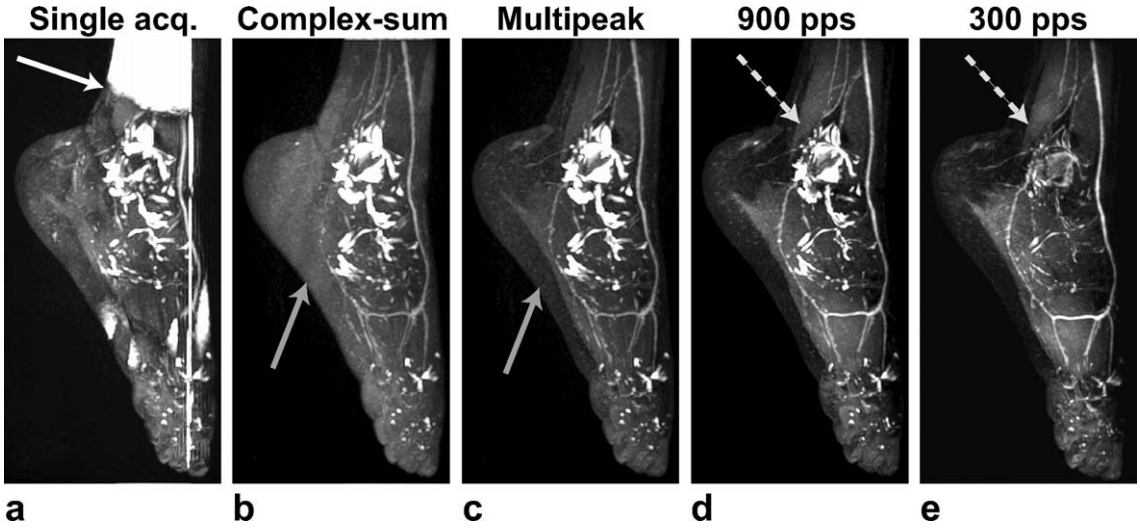

Figure 5. Maximum-intensity projections (MIPs) of IDEAL bSSFP foot angiograms, demonstrating the effect of the individual elements in the proposed strategy. **a**: The banding artifacts in bSSFP images can result in the failure of the IDEAL fat/water separation. **b**: These artifacts are removed with complex-sum bSSFP. **c**: Improved fat suppression is achieved with the multipeak IDEAL reconstruction. **d**: The joint-fluid signal is reduced with magnetization preparation (900 phase encodes acquired per each *k*-space segment). **e**: More frequent preparation (300 encodes per segment) improves the fluid suppression.

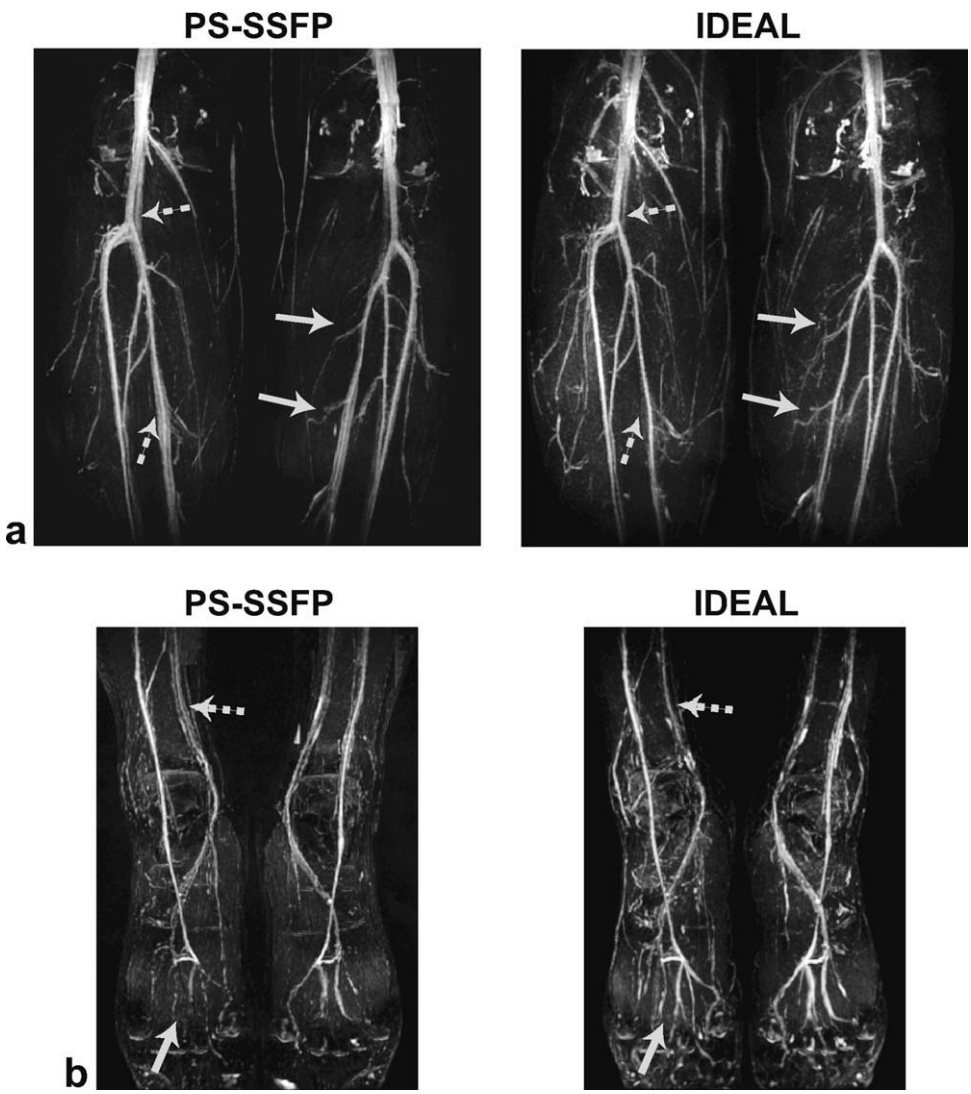

Figure 6. MIPs of (**a**) the lower-leg and (**b**) the foot angiograms produced with PS-SSFP and IDEAL bSSFP. Because IDEAL has reduced sensitivity to partial-volume effects compared with PS-SSFP, it enhances small vessel depiction (solid arrows). The longer TRs used for IDEAL decrease the T_2 of venous blood and yield improved venous suppression (dashed arrows).

Table 2
The Arterial/Venous (A/V) and Blood/Muscle (B/M) Contrast, and the Arterial Blood SNR Measurements on Peripheral Angiograms Along With *P* Values From Student's t-Tests[a]

	PS-SSFP	IDEAL	*P* value
A/V_1	1.29 ± 0.04	1.62 ± 0.02	< 0.10
A/V_2	1.23 ± 0.09	1.51 ± 0.17	< 0.10
B/M_1	3.65 ± 0.40	2.75 ± 0.31	< 0.10
B/M_2	2.66 ± 0.09	2.15 ± 0.30	> 0.10
SNR_1	16.76 ± 2.43	19.77 ± 1.76	< 0.10
SNR_2	13.76 ± 2.57	19.51 ± 1.71	< 0.10

[a]The superscripts denote the first and second sets of measurements performed on the anterior tibial and dorsalis pedis arteries, respectively.

venous suppression due to its longer TR compared with PS-SSFP (17,18). The arterial/venous and blood/muscle contrast as well as blood SNR measurements are listed in Table 2. The increased blood/muscle contrast with PS-SSFP may be attributed to the increased magnetization-transfer effect due to its shorter TR (22). On the other hand, IDEAL achieves 24% higher arterial/venous contrast than PS-SSFP, which closely matches the theoretical estimate (25%). IDEAL also improves the SNR by 29% on average over PS-SSFP. The image SNR is a complicated function of the echo-spacing, the fat/water fraction at a given voxel, the alignment of *k*-space locations with the transient signal, and the extent of the over-sampled *k*-space region. However, a simplified estimate of the SNR improvement with IDEAL is 22% (slightly lower than the measured value), considering the number of echoes and the acceleration factors. All contrast and SNR comparisons between PS-SSFP and IDEAL were found to be statistically significant ($P < 0.10$) except for one (i.e., the blood/muscle contrast on the dorsalis pedis arteries).

Figure 7 displays the IDEAL bSSFP angiograms of the entire lower extremities produced in three stations: the thigh, calf, and foot. High levels of blood/muscle and arterial/venous contrast can be maintained throughout the extremities, and the joint-fluid signal is sufficiently suppressed. High isotropic resolution of the angiograms enables the detailed depiction of the vasculature.

DISCUSSION

The proposed technique produces flow-independent peripheral angiograms without contrast agents by suppressing the signal from fat, synovial fluid, muscle, and veins. Because this strategy effectively deals with field inhomogeneity and partial-volume effects, high-resolution vessel images can be acquired with uniform angiographic contrast over the entire lower extremities. Other angiography applications could potentially benefit from the reliable contrast of this technique.

For most of the previously proposed bSSFP-FIA methods, fat suppression is compromised due to field inhomogeneity (12–16). While techniques that modify the bSSFP profile are not compatible with complex-sum bSSFP, PS-SSFP and IDEAL can be used to process complex-sum datasets with improved immunity against off-resonance. PS-SSFP is simpler and faster,

Figure 7. IDEAL bSSFP angiograms of the entire lower extremities were produced in three stations: the thigh, calf, and foot respectively. Detailed depiction of the peripheral vasculature is achieved through high-resolution acquisitions and reliable background suppression. The "gray" background in the images is due to the residual signal from peripheral muscle tissue, which is closer to the coils than the deep arteries. This creates an inadvertent increase in the muscle signal.

but IDEAL offers improved venous suppression due to its longer TRs. Although PS-SSFP could also be implemented with longer TRs, IDEAL enhances the small-vessel visibility with a fat suppression more robust against partial-volume effects. This can be important in the extremities, where partial-volume effects are significant and deep veins are adjacent to the arteries. The long-TR bSSFP sequence also reduces the SAR and hence allows larger-tip-angle excitations.

Several promising flow-dependent techniques have recently been proposed for MRA in the extremities, such as half-Fourier fast spin echo (FSE) imaging with flow-spoiling pulses (39), and flow-sensitive-dephasing (FSD)-prepared bSSFP (40). Both techniques subtract images collected during diastolic and systolic phases of the cardiac cycle, and can yield higher blood-to-background contrast than the IDEAL approach. However, trigger delays and blood flow in non-readout directions can both lead to suboptimal background suppression and blood-signal loss. Furthermore, the FSD technique suffers from bSSFP banding artifacts at large FOVs and high field strengths. In contrast, the IDEAL method is robust against field inhomogeneity due to complex-sum bSSFP.

Limitations

The complex-sum bSSFP profiles have significantly improved flatness compared with the individual phase-cycled acquisitions. Therefore, the misalignment of the fat and water profiles does not pose critical problems. However, for optimal performance, these profiles should be aligned by using TR values that are integer multiples of 4.6 ms. This could further enhance the uniformity of fat suppression in the IDEAL images.

Because complex-sum bSSFP is implemented with two sequential acquisitions, patient motion can lead to image artifacts. Alternatively, the *k*-space segments of the (0–0)° and (0–180)° phase-cycled datasets could be collected in an interleaved manner. Although significant artifacts were not observed in the lower extremities, considerable motion might be experienced with uncooperative or older patients, or during abdominal imaging. In these cases, image registration or improved correction with navigators might be necessary to maintain high image quality.

The reception sensitivity is higher for peripheral tissues that are closer to the coils than the deep arteries. As a result of this uneven magnitude weighting, increased background signal will be seen in MIPs. Although we did not observe any vessels to be obscured due to this effect, the quality of the MIPs could potentially be improved with intensity correction algorithms for nonuniform coil sensitivities.

Potential Improvements

In this work, ARC parallel imaging is used to improve the quality of the angiograms without further increases in the scan time. Although the acquisitions for noncontrast-enhanced bSSFP angiograms can also be accelerated with compressed sensing (CS) (41), the use of CS with IDEAL is nontrivial. Because the original data have bright fat signal, the images are not as sparse and the achievable acceleration factor is reduced. On the other hand, IDEAL reconstructions will be adversely affected if the undersampling artifacts are not removed first. Alternatively, the two problems may be jointly solved if IDEAL reconstructions are modified to enforce the sparsity of the resulting water images.

Full peripheral coverage might require a small degree of overlap between FOVs of adjacent stations. Although reasonable scan times were maintained in this work through parallel imaging, shorter scans might hence improve the clinical utility of the sequence. Higher acceleration factors can be achieved with the improved SNR efficiency at higher field strengths (e.g., 3 T) and/or the use of dedicated coils with a higher number of elements such as full-leg coils.

Imaging at 3 T can also be desirable for improving the arterial/venous contrast (17,18). The complex-sum bSSFP method will continue to reliably suppress banding artifacts. However, because the fat-water frequency separation doubles at 3 T, the IDEAL echo spacing needs to be halved to maintain the same phase difference as in the 1.5 T case. We can simply acquire one echo per TR to shorten the spacing, but this decreases the acquisition duty cycle and the resulting scan efficiency. We can instead use bipolar gradients with reversed polarities if we correct for the resulting *k*-space misalignments (26).

In conclusion, magnetization-prepared complex-sum bSSFP with IDEAL fat/water separation creates reliable angiographic contrast by successfully suppressing the background signals, and reducing the sensitivity to partial-volume effects and field inhomogeneity. Because the proposed technique is flow-independent, high-spatial-resolution angiograms can be produced over large FOVs in the extremities without compromising contrast.

REFERENCES

1. Missouris CG, Buckenham T, Cappuccio FP, MacGregor GA. Renal artery stenosis: a common and important problem in patients with peripheral vascular disease. Am J Med 1994;96:10–14.
2. Kanal E, Barkovich AJ, Bell C, et al. ACR guidance document for safe MR practices: 2007. AJR Am J Roentgenol 2007;188: 1447–1474.
3. Thomsen HS. Nephrogenic systemic fibrosis: a serious late adverse reaction to gadodiamide. Eur Radiol 2006;16:2619–2621.
4. Miyazaki M, Lee VS. Nonenhanced MR angiography. Radiology 2008;248:20–43.
5. Axel L, Morton D. MR flow imaging by velocity-compensated/uncompensated difference images. J Comput Assist Tomogr 1987;11:31–34.
6. Dumoulin CL, Cline HE, Souza PS, Wagle W, Walker MF. Three-dimensional time-of-flight magnetic resonance angiography using spin saturation. Magn Reson Med 1989;11:35–46.
7. Miyazaki M, Sugiura S, Tateishi F, Wada H, Kassai Y, Abe H. Non-contrast-enhanced MR angiography using 3D ECG-synchronized half-Fourier fast spin echo. J Magn Reson Imaging 2000;12:776–783.
8. Wright GA, Nishimura DG, Macovski A. Flow-independent magnetic resonance projection angiography. Magn Reson Med 1991; 17:126–140.

9. Brittain JH, Olcott EW, Szuba A, et al. Three-dimensional flow-independent peripheral angiography. Magn Reson Med 1997;38: 343–354.
10. Koktzoglou I, Edelman RR. STAR and STARFIRE for flow-dependent and flow-independent noncontrast carotid angiography. Magn Reson Med 2009;61:117–124.
11. Carr HY. Steady-state free precession in nuclear magnetic resonance. Phys Rev 1958;112:1693–1701.
12. Brittain JH, Shimakawa A, Wright GA, et al. Non-contrast-enhanced flow-independent, 3D peripheral angiography using steady-state free precession at 3T. In: Proceedings of the 11th Annual Meeting of ISMRM, Toronto, 2003. (abstract 1710).
13. Brittain JH, Reeder S, Shimakawa A, et al. Non-contrast-enhanced angiography at 3T using SSFP and "Dixon" fat-water separation. In: Proceedings of the 12th Annual Meeting of ISMRM, Kyoto, 2004. (abstract 12).
14. Bangerter NK, Hargreaves BA, Brittain JH, Hu B, Vasanawala SS, Nishimura DG. 3D fluid-suppressed T2-prep flow-independent angiography using balanced SSFP. In: Proceedings of the 12th Annual Meeting of ISMRM, Kyoto, 2004. (abstract 11).
15. Çukur T, Lee JH, Bangerter NK, Hargreaves BA, Nishimura DG. Non-contrast-enhanced flow-independent peripheral MR angiography with balanced SSFP. Magn Reson Med 2009;61:1533–1539.
16. Stafford RB, Sabati M, Mahallati H, Frayne R. 3D non-contrast-enhanced MR angiography with balanced steady-state free precession Dixon method. Magn Reson Med 2008;59:430–433.
17. Dharmakumar R, Hong J, Brittain JH, Plewes DP, Wright GA. Oxygen-sensitive contrast in blood for steady-state free precession imaging. Magn Reson Med 2005;53:574–583.
18. Brittain JH, Shimakawa A, Johnson J, et al. Non-contrast-enhanced MR angiography at 3.0T: improved arterial-venous contrast with increased TR. In: Proceedings of the 13th Annual Meeting of ISMRM, Miami Beach, 2005. (abstract 1708).
19. Reeder SB, Wen Z, Yu H, et al. Multicoil Dixon chemical species separation with an iterative least squares estimation method. Magn Reson Med 2004;51:35–45.
20. Reeder SB, Pineda AR, Wen Z, et al. Iterative decomposition of water and fat with echo asymmetry and least-squares estimation (IDEAL): application with fast spin-echo imaging. Magn Reson Med 2005;54:636–644.
21. Vasanawala SS, Pauly JM, Nishimura DG. Linear combination steady-state free precession MRI. Magn Reson Med 2000;43:82–90.
22. Bieri O, Scheffler K. On the origin of apparent low tissue signals in balanced SSFP. Magn Reson Med 2006;56:1067–1074.
23. Hong JA, Dharmakumar R, Brittain JH, Wright GA. A comparative study of oxygen-sensitive contrast between femoral artery and vein in spin-echo and balanced steady-state free precession imaging. In: Proceedings of the 12th Annual Meeting of ISMRM, Kyoto, 2004. (abstract 2322).
24. Reeder SB, Markl M, Yu H, Hellinger JC, Herfkens RJ, Pelc NJ. Cardiac CINE imaging with IDEAL water-fat separation and steady-state free precession. J Magn Reson Imaging 2005;22:44–52.
25. Feinberg DA, Turner R, Jakab PD, Kienlin MV. Echo-planar imaging with asymmetric gradient modulation and inner-volume excitation. Magn Reson Med 1990;13:162–169.
26. Lu W, Yu H, Shimakawa A, Alley M, Reeder SB, Hargreaves BA. Water-fat separation with bipolar multiecho sequences. Magn Reson Med 2008;60:198–209.
27. Yu H, Shimakawa A, McKenzie CA, Brodsky E, Brittain JH, Reeder SB. Multiecho water-fat separation and simultaneous r2* estimation with multifrequency fat spectrum modeling. Magn Reson Med 2008;60:1122–1134.
28. Kim H, Pinus AB, Wang J, Murphy PS, Constable RT. On the application of chemical shift-based multipoint water-fat separation methods in balanced SSFP imaging. Magn Reson Med 2007; 58:413–418.
29. Bernstein MA, King KF, Zhou XJ. Handbook of MRI pulse sequences. 1st edition. Burlington, MA: Elsevier Academic Press; 2004.
30. Hwang KP, Ward HA, Polzin JA, Ma J. Phase cycled steady state free precession with multi-point fat-water separation. In: Proceedings of the 12th Annual Meeting of ISMRM, Kyoto, 2004. (abstract 268).
31. Silver MS, Joseph RI, Hoult DI. Highly selective $\pi/2$ and π pulse generation. J Magn Reson 1984;59:347–351.
32. Nezafat R, Ouwerkerk R, Derbyshire AJ, Stuber M, McVeigh ER. Spectrally selective B1-insensitive T2 magnetization preparation sequence. Magn Reson Med 2009;61:1326–1335.
33. Le Roux P. Simplified model and stabilization of SSFP sequences. J Magn Reson 2003;163:23–37.
34. Spincemaille P, Nguyen TD, Wang Y. View ordering for magnetization prepared steady state free precession acquisition: Application in contrast-enhanced MR angiography. Magn Reson Med 2004;52:461–466.
35. Wilman AH, Riederer SJ. Performance of an elliptical centric view order for signal enhancement and motion artifact suppression in breath-hold three-dimensional gradient echo imaging. Magn Reson Med 1997;38:793–802.
36. Gold GE, Han E, Stainsby J, Wright GA, Brittain JH, Beaulieu CF. Musculoskeletal MRI at 3.0 T: relaxation times and image contrast. AJR Am J Roentgenol 2004;183:343–351.
37. Brau ACS, Beatty PJ, Skare S, Bammer R. Comparison of reconstruction accuracy and efficiency among autocalibrating data-driven parallel imaging methods. Magn Reson Med 2008;59: 382–395.
38. Hargreaves BA, Bangerter NK, Vasanawala SS, Shimakawa A, Brittain JH, Nishimura DG. Dual-acquisition phase-sensitive SSFP water-fat separation. Magn Reson Imaging 2006;24: 113–122.
39. Miyazaki M, Takai H, Sugiura S, Wada H, Kuwahara R, Urata J. Peripheral MR angiography: separation of arteries from veins with flow-spoiled gradient pulses in electrocardiography-triggered three-dimensional half-Fourier fast spin-echo imaging. Radiology 2003;227:890–896.
40. Fan Z, Sheehan J, Bi X, Liu X, Carr J, Li D. 3D noncontrast MR angiography of the distal lower extremities using flow-sensitive dephasing (FSD)-prepared balanced SSFP. Magn Reson Med 2009;62:1523–1532.
41. Çukur T, Lustig M, Nishimura DG. Improving non-contrast-enhanced steady-state free precession angiography with compressed sensing. Magn Reson Med 2009;61:1122–1131.